Phase Behavior and Dewetting for Polymer Blend Films Studied by In Situ AFM and XPS: From Thin to Ultrathin Films

Yonggui Liao,[†,§] Jichun You,[†,§] Tongfei Shi,*[,†] Lijia An,*[,†] and Pradip Kumar Dutta[‡]

State Key Laboratory of Polymer Physics and Chemistry, Changchun Institute of Applied Chemistry, Chinese Academy of Sciences, Changchun 130022, People's Republic of China, and Department of Chemistry, M. N. National Institute of Technology, Allahabad-211 004, India

Received June 14, 2007. In Final Form: August 19, 2007

In this work, the film thickness (l_0) effect on the phase and dewetting behaviors of the blend film of poly(methyl methacrylate)/poly(styrene-*ran*-acrylonitrile) (PMMA/SAN) has been studied by in situ atomic force microscopy (AFM) and X-ray photoelectron spectroscopy (XPS). The thinner film shows the more compatibility of the blend, and the phase separation of the film occurs at $l_0 > 5R_g$ (radius of gyration). An initially time-independent q^*, the characteristic wavenumber of the phase image, which is in good agreement of Cahn's linearized theory for the early stage of spinodal decomposition, has been obtained in real space and discussed in detail. For $5R_g > l_0 > 3R_g$, a "pseudo-dewetting/(phase separation + wetting)" behavior occurs, where the pseudo-wetting is driven by the concentration fluctuation mechanism. For $l_0 < 3R_g$, a "real dewetting/(phase separation + wetting)" behavior occurs.

Introduction

Using phase separation in thin polymer blend films, plenty of structures, which are important for many applications ranging from microelectronic device fabrication (e.g., lithography) to biomedical (e.g., drug-released capsule), can be tuned conveniently.[1,2] It is well known that phase separation may occur either by nucleation and growth mechanism (N&G) or by spinodal decomposition mechanism (SD) after a blend is abruptly quenched into a metastable or unstable region. As for the SD phase separation, it can be divided into three stages, that is, the early, intermediate, and late stages. In the early stage, the phase behavior is well described by Cahn's linearized theory.[3,4] The characteristic wavelength of composition fluctuation wave (q^*) is almost independent of annealing time (t), while its amplitude increases with t. In the intermediate and the late stages, the power law $q^* \approx t^{-n}$, where n is the power exponent, is often used to describe the time evolution of phase domains. A lot of theories and simulations[5−15] and many experiments (especially various scattering techniques)[16−27] have been reported on the power law of the phase separation of polymer blends since Lifshitz and Slyozov[28] obtained an $n = 1/3$ due to diffusion effects for the intermediate stage and Siggia[29] obtained an $n = 1$ with the proposal of tube hydrodynamic instability for the late stage. In a previous work, using in situ atomic force microscopy (AFM), which has been employed in many studies,[30−41] we have investigated the kinetics of surface phase separation of thin films of poly(methyl methacrylate)/poly(styrene-*ran*-acrylonitrile) (PMMA/SAN) blend, which shows a typical lower critical solution temperature (LCST) behavior in the bulk.[42] The results showed that the critical surface phase separation temperature for thin film of 50/50 (wt %) with the thickness of $14.5R_g$ (radius of gyration) was ∼165 °C. From the scaling power exponent n, two distinct regimes with $n \approx 0.13$ and $\sim 1/3$ were found through the whole investigated time scale in two-phase regions at 175 and 185 °C. However, the early

* Corresponding authors. Tel.: +86-431-5262137 (T.S.), +86-431-5262206 (L.A.). Fax: +86-431-5262969 (T.S.), +86-431-5685653 (L.A.). E-mail: tfshi@ciac.jl.cn (T.S.), ljan@ciac.jl.cn (L.A.).

† Chinese Academy of Sciences.

‡ M. N. National Institute of Technology.

§ Ph.D student of the Graduate School of the Chinese Academy of Sciences. These authors contributed equally to this work.

(1) Binder, K. *Adv. Polym. Sci.* **1999**, *138*, 1.
(2) Budkowski, A. *Adv. Polym. Sci.* **1999**, *148*, 1.
(3) Cahn, J. W.; Hilliard, J. E. *J. Chem. Phys.* **1958**, *28*, 258.
(4) Cook, H. E. *Acta Metall.* **1970**, *18*, 297.
(5) Puri, S.; Binder, K. *Phys. Rev. Lett.* **2001**, *86*, 1797.
(6) Tanaka, H.; Araki, T. *Phys. Rev. Lett.* **1998**, *81*, 389.
(7) Liu, H.; Bhattacharya, A.; Chakrabarti, A. *J. Chem. Phys.* **1999**, *111*, 11183.
(8) Thompson, P. A.; Grest, G. S.; Robbins, M. O. *Phys. Rev. Lett.* **1992**, *68*, 3448.
(9) Bhattacharya, A.; Mahanti, S. D.; Chakrabarti, A. *Phys. Rev. Lett.* **1998**, *80*, 333.
(10) Colombani, J.; Bert, J. *Phys. Rev. E* **2004**, *69*, 011402.
(11) Fialkowski, M.; Aksimentive, A.; Holyst, R. *Phys. Rev. Lett.* **2001**, *86*, 240.
(12) Troian, S. M. *Phys. Rev. Lett.* **1993**, *71*, 1399.
(13) Laradji, M.; Toxvaerd, S.; Mouritsen, O. G. *Phys. Rev. Lett.* **1996**, *77*, 2253.
(14) Taniguchi, T.; Onuki, A. *Phys. Rev. Lett.* **1996**, *77*, 4910.
(15) Bates, F. S.; Wiltzius, P. *J. Chem. Phys.* **1989**, *91*, 3258.
(16) Kubota, K.; Kuwahara, N. *Phys. Rev. Lett.* **1992**, *68*, 197.
(17) Sung, L.; Karim, A.; Douglas, J. F.; Han, C. C. *Phys. Rev. Lett.* **1996**, *76*, 4368.
(18) Bruder, F.; Brenn, R. *Phys. Rev. Lett.* **1992**, *69*, 624.
(19) Shi, B. Q.; Harrison, C.; Cumming, A. *Phys. Rev. Lett.* **1993**, *70*, 206.
(20) Wiltzius, P.; Cumming, A. *Phys. Rev. Lett.* **1991**, *66*, 3000.
(21) Piazza, R.; Pierno, M.; Vignati, E.; Venturoli, G.; Francia, F.; Mallardi, A.; Palazzo, G. *Phys. Rev. Lett.* **2003**, *90*, 208101.
(22) Tanaka, H. *Phys. Rev. Lett.* **1994**, *72*, 3690.
(23) Haas, C. K.; Torkelson, J. M. *Phys. Rev. Lett.* **1995**, *75*, 3134.
(24) Takeno, H.; Hashimoto, T. *J. Chem. Phys.* **1998**, *108*, 1225.
(25) Wang, H.; Composto, R. J. *J. Chem. Phys.* **2000**, *113*, 10386.
(26) Wang, H.; Composto, R. J. *Interface Sci.* **2003**, *11*, 237.
(27) An, N. R.; Yang, Y. M.; Dong, L. S. *Macromolecules* **2007**, *40*, 306.
(28) Lifshitz, I. M.; Slyozov, V. V. *J. Phys. Chem. Solids* **1961**, *19*, 35.
(29) Siggia, E. D. *Phys. Rev. A* **1979**, *20*, 595.
(30) Xie, A. F.; Yamada, R.; Gewirth, A. A.; Granick, S. *Phys. Rev. Lett.* **2002**, *89*, 246103.
(31) Noy, A.; Zepeda, S.; Orme, C. A.; Yeh, Y.; Yoreo, J. J. D. *J. Am. Chem. Soc.* **2003**, *125*, 1356.
(32) Magonov, S. N.; Yerina, N. A. *Langmuir* **2003**, *19*, 500.
(33) Schönherr, H.; Waymouth, R. M.; Frank, C. W. *Macromolecules* **2003**, *36*, 2412.
(34) Chan, C. M.; Li, L. *Adv. Polym. Sci.* **2005**, *188*, 1.
(35) Roiter, Y.; Minko, S. *J. Am. Chem. Soc.* **2005**, *127*, 15688.
(36) Organ, S. J.; Hobbs, J. K.; Miles, M. J. *Macromolecules* **2004**, *37*, 4562.
(37) Loos, J. *Adv. Mater.* **2005**, *17*, 1821.
(38) Fu, G.; Qiu, S. R.; Orme, C. A.; Morse, D. E.; De Yoreo, J. J. *Adv. Mater.* **2005**, *17*, 2678.
(39) Wiedemair, J.; Serpe, M. J.; Kim, J.; Masson, J. F.; Lyon, L. A.; Mizaikoff, B.; Kranz, C. *Langmuir* **2007**, *23*, 130.
(40) Kumaki, J.; Kawauchi, T.; Yashima, E. *Macromolecules* **2006**, *39*, 1209.
(41) Li, B. S.; Sattin, B. D.; Goh, M. C. *Nano Lett.* **2006**, *6*, 1474.
(42) Liao, Y. G.; Su, Z. H.; Ye, X. G.; Li, Y. Q.; You, J. C.; Shi, T. F.; An, L. J. *Macromolecules* **2005**, *38*, 211.

10.1021/la701761p CCC: $37.00
Published on Web 09/26/2007

stage with $n \approx 0$ has not been obtained yet. It is well known that confinement makes the polymer blend more compatible.[43−45] Zhu and co-workers had reported the confinement-induced miscibility of PS/P(S-co-MMA)/PMMA thin film on a cleaned silicon substrate.[46] While the films were annealed abundantly, the effect of the film thickness of the blend of PS and the copolymer on PMMA on the miscibility was investigated. They found that the micelles remained after the dissolution of the PS phase on the surface of the PMMA layer for thick PS layers, while the two homopolymers completely mixed when the PS layer thickness was less than the size of the bulk micelle diameter.

In addition, the stability of polymer films is important for fundamental understanding of mean field theories of wetting and for practical applications ranging from biophysics and coatings to lithography.[47] The polymers have been employed to study the dewetting due to the mass conservation for their very low vapor pressure and the time resolution for their low mobility.[48] Although there have been many reports on dewetting of polymer films, most of them focused on single-component films on solid substrates,[48−54] or one component on top of another.[55,56] Only few studies have been reported on the thin blend films in the phase-separated regions.[26,57−60] The results suggested the formation of bilayer via phase separation, followed by the dewetting of the upper layer relative to the other, which we called "(phase separation + bilayer)/dewetting" mechanism. In another previous work,[61] by means of in situ AFM technique, we have reported the complex behaviors including dewetting and phase separation in the ultrathin blend film of PMMA/SAN (thickness $\sim R_g$). In the miscible region (i.e., at 155 °C), a "spinodal-like" dewetting driven by a composition fluctuation[62,63] occurred. A binary miscible polymer blend on a solid substrate, which can attract one component preferentially, can form a homogeneous thin (or ultrathin) film during spin-coating because the solvent evaporates too fast to reconstruct the polymer chains enough. However, when the film is heated to above its glass transition temperature (T_g), one component will diffuse to the substrate with the preferential interaction between them. A concentration gradient across the film then forms. A composition fluctuation along the surface can be created because this diffusion cannot occur precisely in the same way over the whole film. Finally, when the amplitude of this fluctuation is enough, the dewetting of the free surface occurs. In the two-phase region (at 175 °C), we observed that the dewetting of the whole film was followed by phase separation in the droplets, coupling with the wetting of the substrate (silicon), where PMMA was extracted due to strong interaction between PMMA and substrate. This so-called "dewetting/(phase separation + wetting)" mechanism was a little different from Wang's proposal of "(phase separation + bilayer)/dewetting" mechanism for the same kind of blend with a similar thickness ($\sim {}^3/_4 R_g$) using ex situ AFM technique.[26]

To precisely control the morphology and structure of polymer blend thin film, it is necessary to understand the phase separation for the thin film (i.e., the early stage of SD) and the transition from the thin film to the ultrathin film where the complex behaviors of wetting/dewetting and phase separation occur. Because of the interplay of chain confinement, wetting versus dewetting, lateral versus vertical phase separation, a complex pattern formation and self-organization, which have great potential applications on phase-separated membranes, micro-electronics, drug-released capsules, nanoreactors, etc., is possible in such thin and ultrathin films. Therefore, in this work, we present first direct evidence for the early stage of surface SD of thin polymer blend films in real space and the discussion on the transition from the thin to the ultrathin films of polymer blend with great detail.

Experimental Section

Materials. Poly(methyl methacrylate) (PMMA, M_w = 387 kg/mol, PD = 3.72, Across) and poly(styrene-*ran*-acrylonitrile) (SAN, 30% AN by mass, M_w = 149 kg/mol, PD = 2.66, Aldrich) were used as received. The glass transition temperatures (T_g) of PMMA and SAN, obtained from a differential scanning calorimeter (Perkin-Elmer Diamond DSC) at an elevated rate of 10 °C/min, were 128.7 and 112.0 °C, respectively.[42]

Sample Preparation. Prior to spin-coating, silicon wafers were boiled in a bath of 100 mL of 80% H_2SO_4, 35 mL of H_2O_2, and 15 mL of deionized water for 15 min and rinsed in deionized water, and then dried with compressed nitrogen.[42,57] The coated thin films of PMMA/SAN blend were kept under vacuum for at least 12 h and then in a dryer after being prepared by spin-coating 0.50×10^{-2}, 0.35×10^{-2}, and 0.25×10^{-2} g/mL 1,2-dichloroethane solution of the blend (50:50 wt %) onto the pretreated silicon wafers. The thickness of films (l_0) as measured by a Bruker D8 Discover X-ray reflectometer was 50.4 ± 0.2, 39.8 ± 1.0, and 22.2 ± 0.2 nm. The larger was the solution concentration, the thicker was the film that formed. The samples were denoted as *S1*, *S2*, *S3*, *S4*, and *S5* for the film with thicknesses of 133.5, 50.4, 39.8, 22.2, and 8.9 nm, respectively.

In Situ Atomic Force Microscopy (AFM) Measurements. The AFM measurements were carried out on a scanning probe microscope (SPA-300HV, Seiko Instruments Inc., Japan) equipped with a temperature-control stage. The temperature reading for the hot stage was calibrated with pure gallium, indium, and tin, whose melting points (T_m) are 30, 156, and 232 °C, respectively. The sample was heated to 115 °C at a rate of 5 °C/min, annealed at that temperature for at least 60 min to remove residual solvent completely, and again heated to 175 °C. A control experiment performed at 115 °C showed that the annealing sample did not cause phase separation or surface roughening (not shown here). The in situ topography and phase images were obtained simultaneously by virtue of a tapping mode AFM at 175 °C under ultrahigh vacuum ($<10^{-4}$ Pa). A silicon tip (purchased from Olympus) with a spring constant of 42 N/m was used. AFM was operated at a scan speed of 2 Hz. To ensure the steadiness of the contrast in the height and phase images and to minimize the influence of height variations on the phase images, the set-point ratio under ultrahigh vacuum was set at 0.96 ± 0.01.[42]

The data of root-mean-square surface smoothness of height (rms_h) and of phase (rms_p) were directly obtained from topography and phase images of a $2 \times 2\ \mu m^2$ area using the commercial software bundled with the AFM to ensure that at least one complete protuberance was included, and the data of characteristic wave-

(43) Kumar, S. K.; Tang, H.; Szleifer, I. *Mol. Phys.* **1994**, *81*, 867.
(44) Rouault, Y.; Baschnagel, J.; Binder, K. *J. Stat. Phys.* **1995**, *80*, 1009.
(45) Flebbe, T.; Dünweg, B.; Binder, K. *J. Phys. II (France)* **1996**, *6*, 667.
(46) Zhu, S.; Liu, Y.; Rafailovich, M. H.; Sokolov, J.; Gersappe, D.; Winesett, D. A.; Ade, H. *Nature* **1999**, *400*, 49.
(47) Geoghegan, M.; Krausch, G. *Prog. Polym. Sci.* **2003**, *28*, 261.
(48) Reiter, G. *Phys. Rev. Lett.* **1992**, *68*, 75.
(49) Xie, R.; Karim, A.; Douglas, J. F.; Han, C. C.; Weiss, A. *Phys. Rev. Lett.* **1998**, *81*, 1251.
(50) Gleiche, M.; Chi, L. F.; Fuchs, H. *Nature* **2000**, *403*, 173.
(51) Higgins, A. M.; Jones, R. A. L. *Nature* **2000**, *404*, 476.
(52) Reiter, G. *Phys. Rev. Lett.* **2001**, *87*, 186101.
(53) Huang, E.; Rockford, L.; Russell, T. P.; Hawker, C. *Nature* **1998**, *395*, 757.
(54) Sehgal, A.; Ferreiro, V.; Douglas, J. F.; Amis, E. J.; Karim, A. *Langmuir* **2002**, *18*, 7041.
(55) Reiter, G.; Auroy, P.; Auvray, L. *Macromolecules* **1996**, *29*, 2150.
(56) Ross, D.; Bonn, D.; Meunier, J. *Nature* **1999**, *400*, 737.
(57) Müller-Buschbaum, P.; O'Neil, S. A.; Affrossman, S.; Stamm, M. *Macromolecules* **1998**, *31*, 5003.
(58) Yerushalmi-Rozen, R.; Kerle, T.; Klein, J. *Science* **1999**, *285*, 1254.
(59) Oron, M.; Kerle, T.; Yerushalmi-Rozen, R.; Klein, J. *Phys. Rev. Lett.* **2004**, *92*, 236104.
(60) Tanaka, K.; Yoon, J. S.; Takahara, A.; Kajiyama, T. *Macromolecules* **1995**, *28*, 934.
(61) Liao, Y. G.; Su, Z. H.; Sun, Z. Y.; Shi, T. F.; An, L. J. *Macromol. Rapid Commun.* **2006**, *27*, 351.
(62) Wensink, K. D. F.; Jérôme, B. *Langmuir* **2002**, *18*, 413.
(63) Sharma, A.; Mittal, J. *Phys. Rev. Lett.* **2002**, *89*, 186101.

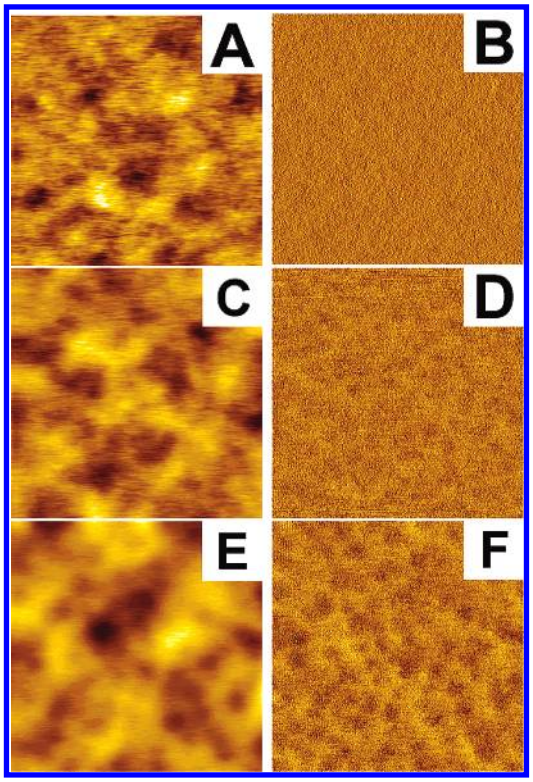

Figure 1. Snapshots of topography (left) and phase (right) images for PMMA/SAN (50:50 wt %) thin film (thickness 50.4 nm, ~5.5R_g) at 175 °C for 8 min (A,B), 150 min (C,D), and 976 min (E,F). The *z*-axes are 2.4 nm (A), 4.1 nm (C), 9.7 nm (E), and 1.8° for all phase images, respectively. The edge length of all images is 2 μm.

numbers, q^*, were computed from the phase image of a 2 × 2 μm^2 area as described in our previous work, where a further spherical average was performed after the routine 2D Fourier transforms (FT).[42,61]

X-ray Photoelectron Spectroscopy (XPS) Measurements. After being annealed at 175 °C in an oven under vacuum for different times, the films were carried out for XPS measurements at room temperature. Signal of Si was determined by a Thermo ESCALAB 250 spectrometer with AL X-ray source ($h\nu$ = 1486.6 eV). The takeoff angle of the X-ray source was 90°. The chemical shift peaks were charge-referenced to the C−C/C−H peak at 284.6 eV. The pressure of sample analysis chamber was about 2.0 × 10^{-7} Pa in course of the spectra.

Results and Discussion

I. Early Stage of Spinodal Decomposition for Thin Film (l_0 = 50.4 nm). Figure 1 shows the snapshots of topography (left) and phase (right) images for a PMMA/SAN (50:50 wt %) thin film with thickness of 50.4 nm (*S2*, ~5.5R_g), after different annealing times at 175 °C. The topography images show that the height increases with the increase of time during annealing. However, the phase images vary with time in a different way. The phase image is homogeneous when the film is annealed for 8 min. From then on, the surface phase separation starts to develop gradually (see the phase image at 150 min annealing, Figure 1D) with separation of two distinct types of regions: darker and lighter ones. Finally, the darker domains are dispersed into the lighter matrices (Figure 1F). For quantitative analysis of the kinetics of surface phase separation, the characteristic wavenumber (q^*) of the phase image is employed in this work. This method has been successfully used in our previous work.[42] The time dependence of q^* is plotted on a log−log scale in Figure 2. Two distinct regimes can be identified clearly. The power exponents n for $q^* \approx t^{-n}$ are 0.01, almost 0, at the early stage,

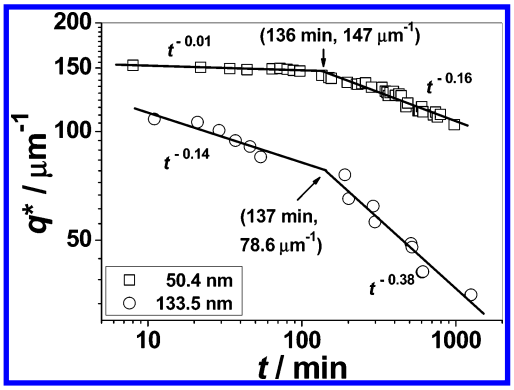

Figure 2. Time dependence of characteristic wavenumbers (q^*) for PMMA/SAN (50:50 wt %) film at 175 °C on a log−log scale. All q^* data are taken from the 2 × 2 μm^2 phase images. Data for the sample with thickness of ~133.5 nm are taken from ref 42.

and 0.16 at the later stage, respectively. Two regimes cross at 136 min with a crossover q^* of 147 μm^{-1}. The $n \approx 0$ that has not been obtained at the early stage for *S1* with thicker film thickness (133.5 nm)[42] indicates the characteristic wavenumber is almost independent of annealing time at early stage. This result is in good agreement with Cahn's linearized theory for the early stage of spinodal decomposition.[3,4] Considered the elevating process from 115 to 175 °C at a rate of 5 °C/min, which passes through the critical temperature of phase separation, the quench is not instantaneous but continuous. Another possible reason for the initially lacking shift of q^* with time is the nonlinear effect of continuous quenching at the early stage of SD.[64] Because long wavelength fluctuations are amplified first during the continuous quench, the initial shift of q^* may be in the opposite direction than at later times, or for some time no shift is detected at all.[64] The n of 0.16 for the later stage is similar to the value of 0.14 for the early regime of the thin film with thickness of 133.5 nm (*S1* ≈ 14.5R_g), at the same annealing temperature (175 °C).[42] As described in our previous work,[42] this slow dynamics of surface phase separation may be found for two reasons. One is the slow diffusion of the component with lower surface tension (PMMA or SAN) to the surface. The other is the chain mobility is reduced due to the two-dimensional geometry constraint of the surface. In a word, not only the lower temperature (for example, at 175 °C relative to 185 °C for *S1*),[42] but also the thinner thickness of the thin film can slow down the kinetics of surface phase separation. It is well known that the confinement makes the polymer blend more compatible.[43−46] In this case, for a fixed temperature (175 °C), we observed that the film thickness is thinner, the quench depth is shallower, and it results in a more compatible blend film, which is shown in the early stage of SD much more easily.

II. Transition from Thin to Ultrathin Blend Films. Figures 3 and 4 show the snapshots of topography (left) and phase (right) images for a PMMA/SAN (50:50 wt %) film with thickness of 39.8 nm (*S3*, ~4.3R_g) and 22.2 nm (*S4*, ~2.4R_g) after different annealing times at 175 °C, respectively. For *S3*, some individual holes form initially (see Figure 3A for annealing time of 19 min), and then gradually grow (Figure 3C for 60 min) and connect each other as a result of separating the droplets (Figure 3E for 554 min). Finally, the droplets are separated entirely and become rounder and rounder (Figure 3G for 1492 min) due to the driving of surface tension. The evolution of topography for *S4* is similar. The film is found to be flat for the annealing time of up to 4 min. Some individual holes are also formed and emerged (Figure 4C

(64) Carmesin, H. O.; Heermann, D. W.; Binder, K. *Z. Phys. B* **1986**, *65*, 89.

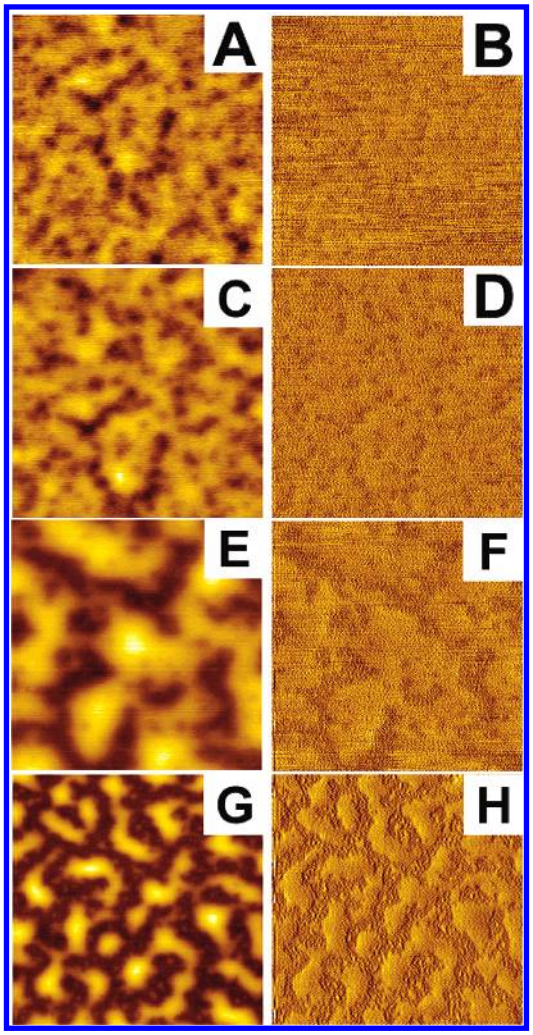

Figure 3. Snapshots of topography (left) and phase (right) images for PMMA/SAN (50:50 wt %) film with thickness of 39.8 nm ($\sim 4.3R_g$) at 175 °C for 19 min (A,B), 60 min (C,D), 554 min (E,F), and 1492 min (G,H). The *z*-axes are 5.5 nm (A), 10.3 nm (C), 30.0 nm (E), 43.8 nm (G), and 3.3° (B,D,F) and 8.0° (H), respectively. The dimensions of (A−F) and of (G,H) are 2×2 μm^2 and 5×5 μm^2.

for 83 min and Figure 4E for 151 min). However, for the whole experiment time scale (Figure 4G for 2709 min), the droplets are not as clear as those in *S3*. It should be noted that the holes and the valley always show a little darker than the matrix or the hill in the phase images. Similarly, the phase contrast for both films is less than 18°, which is similar to the value of ∼10° for the phase contrast between pure PMMA and SAN (where PMMA shows a little darker).[42] These results are slightly different from those obtained from the ultrathin film with thickness of 8.9 nm (*S5*, $\sim R_g$) in our previous work.[61] In that case, the phase contrast increases rapidly and reaches more than 110° for 14 min. This large phase contrast is due to the large difference of viscoelasticity between the liquid polymer melt and the solid silicon substrate. In the phase images, the valley shows a transition from darker to lighter.

To quantitatively analyze the evolution of PMMA/SAN blend films with different thicknesses during annealing, the root-mean-square of height (rms_h) and that of phase (rms_p) are introduced. The time dependence of rms_h and rms_p is shown in Figure 5. Although all rms_h's increase with a power law at the early stage, the power exponents are extremely different. It is only ∼0.18 for *S1* and *S2*. However, it is more than twice that for the other three samples. It is about 0.47 and 0.37 for *S3* and *S4*, and *S5*,

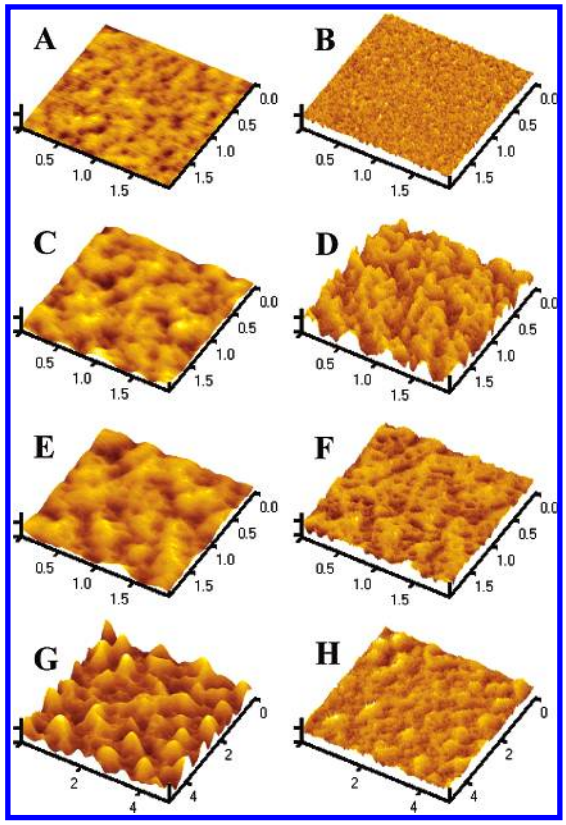

Figure 4. Snapshots of topography (left) and phase (right) images for PMMA/SAN (50:50 wt %) film with thickness of 22.2 nm ($\sim 2.4R_g$) at 175 °C for 4 min (A,B), 83 min (C,D), 151 min (E,F), and 2709 min (G,H). The *z*-axes are 35.0 nm for all topography images and 17.0° for all phase images, respectively. The dimensions of (A−F) and of (G,H) are 2×2 μm^2 and 5×5 μm^2.

respectively. After the power law behavior at the early stage, the rms_h gradually reaches a plateau for the thinner films and goes into another faster power law ($t^{0.45}$) regime for the thicker films, respectively. This indicates that the thinner films (*S3*, *S4*, and *S5*) undergo behaviors different from those of the thicker ones (*S1* and *S2*). As mentioned above, only phase separation has been observed for the thicker films during annealing. For the ultrathin film, *S5*, however, a complex "dewetting/(phase separation + wetting)" behavior occurs. Therefore, one can believe that the thinner films experience dewetting after abruptly jumping to 175 °C, which is ∼60 °C higher than the glass transition temperatures for PMMA and SAN.

The time dependence of rms_p (Figure 5B) and the silicon concentration of the sample surface (Figure 6) can supply further powerful evidence. The rms_p's for *S1*, *S2*, and *S3* always remain at a very low value, as low as 0.3°−0.5°. Such a low value may be due to the similar kind of viscoelasticity as observed for liquid PMMA and SAN. However, the rms_p's for *S4* and *S5* show a different behavior. It rapidly increases in a short time and reaches a maximum, which is ∼2.8° for *S4* and 36° for *S5*, respectively. It decreases to a plateau gradually. Finally, it rapidly drops down to a low value (<1.0°) similar to that of *S1* (*S2* and *S3*). By means of X-ray photoelectron spectroscopy (XPS), we can obtain the silicon concentration of the sample surface, a direct evidence for the coverage of the silicon substrate by the polymer blend films. It almost remains at a low value, less than 5%, for *S2* and *S3* (Figure 6), which indicates that the substrate can be covered by polymers for these two samples only. However, for *S4* and *S5*, it rapidly increases within several hours and then keeps this high value (∼9% for *S4* and ∼36% for *S5*) for the rest of the annealing time.

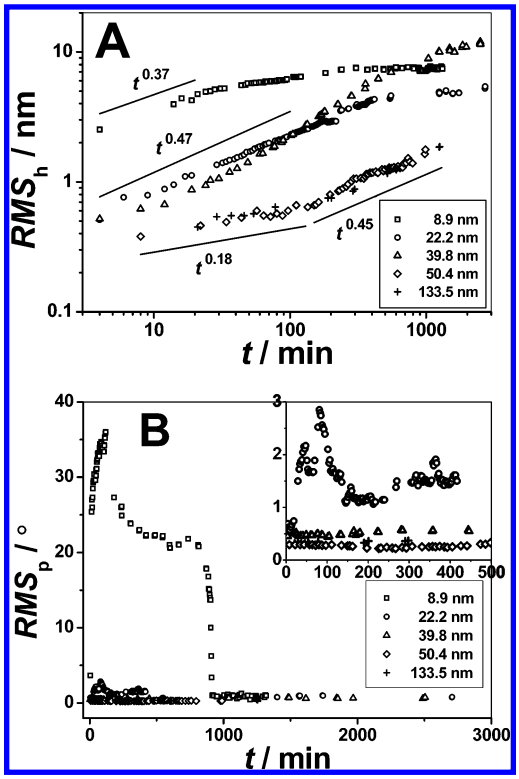

Figure 5. Time dependence of (A) the root-mean-square of height (rms_h) and (B) the root-mean-square of phase (rms_p) of a $2 \times 2\ \mu m^2$ image at 175 °C. The inset shows rms_p within 500 min. Data for the samples with thicknesses of 133.5 and 8.9 nm are taken from refs 42 and 61, respectively.

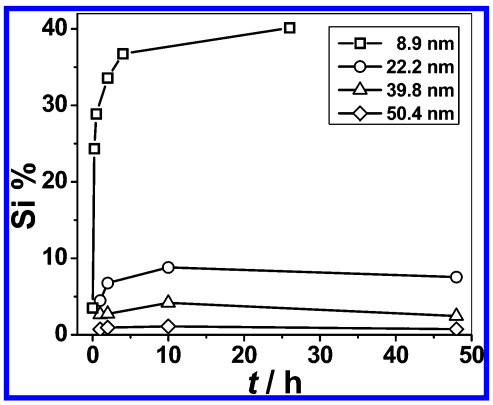

Figure 6. Time dependence of silicon atomic concentration for PMMA/SAN (50:50 wt %) film after different annealing times at 175 °C.

In the two-phase region (175 °C), as compared to a "simple" phase separation for *S1* and *S2* (film thickness $l_0 > 5R_g$), a much more complex behavior is observed in a thinner film ($l_0 < 5R_g$). This behavior includes wetting, dewetting, and phase separation, etc. As reported in our previous work,[61] the ultrathin blend film (*S5*, $l_0 \approx R_g$) undergoes a "dewetting/(phase separation + wetting)" behavior. The ultrathin film thoroughly dewets the solid substrate, and then the droplet inside experiences the phase separation coupling with the wetting of PMMA onto the substrate. Although the silicon concentration obtained from XPS is still very high for annealing time of 26 h, this may be because the penetration depth of XPS is a little larger than that of AFM with a very weak loaded force in this work. Under conditions of Al-α X-ray resource and the perpendicular takeoff angle in this work, the penetration depth for common polymers (say PMMA) is 4−5 nm. The tip for AFM cannot "detect" the solid silicon substrate with a sub-R_g coverage of polymer fluid while the XPS really "detects". Although a bigger takeoff angle for the detector of XPS can give us a thinner surface analysis, the contact angle of the droplet, as described by Sehgal et al.,[54] can easily be estimated at 8°−15°. Thus, a very big detecting angle, which is required in a very thin as well as sub-R_g, cannot be obtained for our case. The behavior of *S4* ($l_0 \approx 2.4R_g$) is similar to that of *S5*; however, it is a little different for S3 ($l_0 \approx 4.5R_g$). The results from the evolution of topography and the time dependence of rms_h indicate that the film really undergoes dewetting initially. Yet both the AFM tip and the XPS cannot detect the solid substrate. Therefore, only a pseudo-dewetting happens for this film. During the removal of the residual solvent at 115 °C (preannealing) and especially the elevating process from 115 to 175 °C, which takes 12 min at a rate of 5 °C/min, there are several nanometers of PMMA, which preferentially attract to the solid substrate and have been strongly attracted and wetted on the substrate. Also, then the rest of the upper polymer blend film dewets on top of the wetting PMMA layer. This early stage is a combination of the dewetting driven by concentration fluctuation and the proposal described by Wang and Composto.[26] This pseudo-dewetting can be understood from two points: On one hand, a sufficient amount of PMMA diffuses to and covers the silicon substrate within a very short time. On the other hand, the driven force of the concentration fluctuation cannot thoroughly penetrate into such a "thick" film ($> 2R_g$) so that only the top layer undergoes dewetting. As a consequence, the droplet experiences phase separation coupling with the further wetting of PMMA onto the substrate. We call this the "pseudo-dewetting/(phase separation + wetting)" mechanism.

Conclusions

In this work, the film thickness (l_0) effect on the phase and dewetting behaviors of the PMMA/SAN blend film has been studied by in situ AFM and XPS. For $l_0 > 5R_g$, only phase separation happens. The thinner is the film, the more compatibility the blend has. An initially time-independent q^*, the characteristic wavenumber of the phase image, which is in good agreement with Cahn's linearized theory for the early stage of spinodal decomposition, has been obtained in real space and discussed in detail. For $5R_g > l_0 > 3R_g$, a "pseudo-dewetting/(phase separation + wetting)" behavior occurs, where the pseudo-wetting is driven by the concentration fluctuation mechanism. For $l_0 < 3R_g$, a "real dewetting/(phase separation + wetting)" behavior occurs. A detailed understanding of the blended polymer film may be helpful for different applications, such as in coating, microlithography, and for nanoreactors.

Acknowledgment. This work is supported by the National Natural Science Foundation of China (20334010, 50503022, 20620120105) Programs and the Fund for Creative Research Groups (50621302), and subsidized by the Special Funds for the National Basic Research Program of China (2003CB615600). L.A. is thankful for support from the National Natural Science Foundation of China (20674086, 50390090) Programs.

LA701761P